Optical telecommunications/Les télécommunications optiques

# The scalability of photonic switches

# Dimensionnement des commutateurs photoniques

Gerd Blau *, Kurt Loesch

*Alcatel Research & Innovation, 70430 Stuttgart, Germany*

Received 3 October 2002

Presented by Guy Laval

## Abstract

The photonic switch deployed in optical cross connects promises transparency and ultra high switch capacity at a per port price that might be competitive to electronic switches in the future. An important factor for cost effectiveness of photonic switches is given through the scaling behaviour of switches at increasing port numbers with respect to insertion loss, footprint and complexity. The well known strictly nonblocking waveguide based switch architectures are compared to the novel single stage crossbar freespace switches and the three dimensional beamsteering switches. New design rules and analytical models based on Gaussian beam propagation theory are given. ***To cite this article: G. Blau, K. Loesch, C. R. Physique 4 (2003).***
© 2003 Académie des sciences/Éditions scientifiques et médicales Elsevier SAS. All rights reserved.

## Résumé

Le commutateur photonique utilisé dans les brasseurs optiques permet la transparence du réseau et une capacité de commutation élevée à un prix compétitif par rapport aux dispositifs électroniques. La rentabilité du commutateur photonique avec l'augmentation du nombre de ports est déterminée par la croissance des pertes d'insertion, de l'empreinte au sol et de la complexité. Le commutateur à base de technologie guide d'onde avec une architecture arborescente est comparé au nouveau type de commutateur cross-bar à base d'ondes libres et au commutateur à déflexion optique en espace libre. De nouvelles règles de conception et nouveaux modèles analytiques basés sur la théorie de propagation des faisceaux Gaussiens sont décrits. ***Pour citer cet article : G. Blau, K. Loesch, C. R. Physique 4 (2003).***
© 2003 Académie des sciences/Éditions scientifiques et médicales Elsevier SAS. Tous droits réservés.

*Keywords:* OXC; DWDM; MEMS; Switch; Gate; Optical; Photonic; Freespace; Waveguide; 3D; Scalability

*Mots-clés :* OXC ; DWDM ; MEMS ; Commutateur ; Gate ; Optique ; Photonique ; Espace libre ; Guide d'onde ; 3D ; Scalabilité

## 1. Introduction

Most long-haul inter-exchange carriers deployed *dense wavelength division multiplexing* (DWDM) technology on their existing fiber links to benefit from the enormous transmission capacity on a single fiber with more than 1 Tbit/s. However, the deployment of DWDM was at the beginning restricted to point-to-point connections or to ring-based topologies. Bandwidth management and active reconfiguration was not performed at the physical/optical layer but at the protocol layer (e.g.,

* Corresponding author.
*E-mail addresses:* gerd.blau@alcatel.de (G. Blau), kurt.loesch@alcatel.de (K. Loesch).

SONET/SDH). Today, the introduction of optical networking at the physical layer promises to give more flexibility to the carrier to build dynamic networks and to provide bandwidth where it is needed.

One of the key components for optical networking is considered to be the *optical cross connect* (OXC). In order to give the optimum flexibility to an optical network, the OXC should be able to interconnect and switch at wavelength level, just as an automated optical distribution frame. In addition, wavelength conversion, grooming, protection switching and regeneration might also be required [1]. No passive optical element can fulfil all of these functions. Electronics, opto-electronics or non-linear optics will always be necessary to allow grooming capabilities or wavelength conversion. However, the key function, which means the configuration of fibers independent from data rate can be done by passive optical elements or also called 'photonic switches'. Waveguide switches, movable mirrors, lenses, gratings with changing periods can be used to influence the direction of light and to couple light from any input single-mode fiber to any output single-mode fiber. The importance of these optical devices for future optical networks has been thoroughly analysed in the past [2]. Since then, some aspects had to be reconsidered after the introduction of transparent optical free-space beam-steering switches, which pushed all known limits with respect to switch capacity and size [3]. The fundamental difference of this type of switch with respect to electrical or active optical devices lies in the nature of light. Optical beams do not interact in linear media when they are crossing, thus blocking of links can not occur for any size of the switch matrix. However, the scaling laws and theoretical limitations in switch capacity of beam-steering switches are not yet fully understood and are subject of this paper.

The major question with respect to the deployment of *photonic switches* is: do these switches become more cost-effective then electrical switches and/or transponders above a certain level of capacity and/or transparency? Concerning opaque switches at data rates $\leqslant 10$ Gbit/sec per optical channel, OXC with electrical core actually seem to persist on the market. However, carriers like to install equipment that is future proof and might be scaled up to higher data rates and higher port counts without exchanging the hardware. This paper intends to summarise the scaling laws of the most common photonic space-switching technologies, to bring up the problems attached to it and to give the upper limits in port counts to be achieved. Concerning 3D free-space switching, a new analytical model is also presented.

## 2. Building larger switches using a network of small switching elements

The smallest switch element is the $1 \times 2$ switch. This switch element is supported by the largest technological base including amongst others *micro electro mechanical systems* (MEMS), *liquid crystals* (LC), *electro-holography* (EH), *acousto-optics* (AO), *electro-optics* (EO) and *thermo-optics* (TO), some of which have the potential to be fast enough for packet or burst switching. One solution in order to scale up a $1 \times 2$ switch to a $M \times M$ OXC is the possibility to interconnect the $1 \times 2$ switch elements by fibers or waveguides. Especially guided-wave based switching elements are suited for increasing the total switch capacity using the *strictly non-blocking* (SN) *active-splitter/active-combiner* (AS/AC) tree-type network [4].

An experimental demonstration was carried out building a $1 \times 8$ guided-wave optical switch using seven $1 \times 2$ polymer/silica *vertically coupled switching* elements (VCS) as basic units [5]. The $1 \times 2$ VCSs are arranged in a tree architecture with three switching stages comprising one, two and four switches respectively. The $1 \times 8$ VCS exhibits an insertion loss of 5–6 dB and an average crosstalk of $-25$ dB. The $1 \times 8$ switch again can be used as a building block for a $M \times M$ OXC. This has been demonstrated in the following experiment using MEMS based $1 \times 2$ elementary switches instead of the VCSs.

An $8 \times 8$ MEMS based all optical switch has been built using a *passive-splitter/active-combiner* (PS/AC) structure [6]. The AC structure is built using eight $8 \times 1$ switches with each of the $8 \times 1$ switches consisting of seven $2 \times 1$ switching elements arranged in a tree structure. The $2 \times 1$ switching elements are based on electrostatically-actuated moving waveguides. The PS structure is interconnected with the AC structure via a perfect shuffle flex-board. A switch capacity of 1.28 Tb/s has been shown within a $16 \times 10$ Gbit/sec. transmission experiment resulting in polarisation dependent loss $<0.3$ dB, wavelength dependent loss $<0.2$ dB and fall and rise time $<1.5$ ms. The resulting insertion loss of less than 18.5 dB is mainly due to the PS structure. Replacing the PS structure by an AS structure will decrease the losses accordingly. The required number of basic $1 \times 2$ switching elements $NSE_{1\times2}$ for this non-blocking AS/AC tree structure is given for $M$ input and $M$ output ports as:

$$NSE_{1\times2} = 2M(M-1). \tag{1}$$

The optical power loss $IL(M)$ scales with the number of switching elements existing within the optical path (stages) according to:

$$IL(M) = 2\log_2(M) \cdot IL_{1\times2}, \tag{2}$$

where $IL_{1\times2}$ corresponds to the loss of each elementary switch supposing equal losses for both switch positions. Eq. (2) neglects the loss that might occur at the waveguide crossings. The number of crossings usually depend on the switch configuration. Loss at waveguide crossings must be kept as small as possible in order to keep total losses and path dependent losses low. Monolithic integration of switches and optical interconnects is often abandoned in favour of fibre shuffle interconnects avoiding

the problems relied to waveguide crossings. Considering the integration density of most photonic $1 \times 2$ switch technologies, it is uncommon to use this architecture with port numbers above $M = 16$ already requiring $NSE = 480$ switching elements and $1.5\,NSE - M = 704$ optical interconnects.

An $8 \times 8$ enhanced passive-select/passive-combiner (PS/PC) switch based on *gain-clamped semiconductor optical amplifiers* (GC-SOAs) has been built, with the GC-SOAs acting as gates in the centre of the PS/PC structure [7]. The eight GC-SOA gate arrays are flip–chip mounted on top of a $SiO_2/Si$ motherboard which integrates a passive $8:1$ power combiner. The complexity of the gate based $M \times M$ switch with $NSE_{SOA} = M^2$ is reduced with respect to the tree-type switch. However, large $M$ values also require a higher level of amplification or cascading with the corresponding increase in electrical power consumption. The optical amplification must compensate the loss of $2 \cdot 10 \log_{10} M$ [dB] of the PS/PC elements, assuming equal power split. Due to this fundamental difference, we will renounce on further scaling law analysis of gate based optical switches in the following.

A mid-sized $M \times M$ or $N \times M$ switch can further be arranged and interconnected in various ways [2]. Concerning SN switches, the three-stage SN *Clos network* has been found to be an effective architecture. If the $N \times M$ photonic switch shows path dependent losses, a Clos network using a specific type of connection pattern, e.g., connecting high loss paths with low loss paths, can be designed resulting in a loss homogenised network [8].

## 3. The 2D freespace cross-bar switch

A typical free-space cross-bar switch can be realised using *digitally controlled mirrors* [9] that are inserted in the optical path at a crossing. The scaling laws of non-blocking cross-bar switches arranged in a 2D matrix are simple. An $M \times M$ switch will require $NSE_{cb} = M^2$ switching elements. The loss between input port $m$ and output port $n$ ($1 \leqslant m, n \leqslant M$) can be calculated using the equation:

$$IL(m, n) = C(m, n) + (m - 1)T + (n - 1)T + R, \tag{3}$$

where $R$ and $T$ correspond to the losses of an elementary switch in the cross and bar state respectively. The term $C(m, n)$ describes the coupling losses. Guided wave based cross bar switches often show high losses and high levels of crosstalk due to losses and scattering in the bar state. The advantage of frees-pace cross-bar switches are evident considering the bar state with zero losses $T = 0$ when no mirror is inserted. The crosstalk level can easily be controlled by adjusting the aperture radius of the collimators and the mirrors. Here, the key parameter is the coupling loss of the collimators which might depend from the optical path and the quality of the mirror surface.

An important parameter is the space required by the switch. In the case of the freespace cross bar switch, the in and output ports are connected by a collimated beam. Any collimated beam starts to diverge after a certain propagation distance, due to the limited beam width and beam aperture. The width of the beam has to be adapted to the distance between the in and output ports using the equations for Gaussian beams [10] in order to keep the coupling losses low. Increasing the numbers of ports in a $M \times M$ switch matrix leads to an increased path-length. Increasing the optical path length $z$ between any in and output port through collimated beams can only be achieved by increasing the width of the beam. A Gaussian beam can be considered as collimated within the *Rayleigh distance* $z_R$. In general, the beam waist $w_0$ is located at the centre between the in and output ports with maximum path length (Fig. 1). The length of the maximum optical path $L_{max}$, which can be set equal to two times the edge length of the switch matrix, is therefore typically chosen to equalise two times $z_R$. The losses and crosstalk are defined by the clipping ratio of the optical beam at the in and output ports. The following calculations all suppose a sufficient size of the beam using $a(z)/w(z) \geqslant \pi/2$ [11] with $a(z)$ being the aperture radius of any optical element located at $z$ and $w(z)$ being the beam waist at the same location. This relatively large aperture with the corresponding clipping loss of $IL = 0.044$ dB should not be considerably reduced in order to avoid diffraction effects and beam spreading behind the aperture leading to crosstalk and coupling loss $> 0.044$ dB. The minimum area of the switch matrix $A$ can be easily calculated when the collimators are aligned along the matrix edge at $z = z_R$ in a linear array with a constant pitch of $p = 2a/f$. The filling factor $f \leqslant 1$ results from manufacturing issues with $f = 1$ being the ideal case. The minimum aperture size of the collimators $a = (\pi/\sqrt{2})w_0$ follows from the assumption that all collimators in the emitting and receiving plane are identical. The minimum matrix size $A$ for a 2D free-space $M \times M$ switch is given by the following equation (neglecting space required for the collimator):

$$A = \left(M \cdot p(M)\right)^2 = \left(\frac{2\pi(M - 0.5)M}{f^2}\lambda\right)^2. \tag{4}$$

The assumption $L_{max} = 2z_R$ leads to a maximum path length variation of ca. $2z_R$ with the corresponding maximum spot size variation in the receiving plane of $w_{max}/w_{min} = \sqrt{2}$. The corresponding path-dependent excess loss is ca. $IL > 0.5$ dB when phase terms are neglected in the overlap integral. Considering a less compact design with $L_{max} > z_R$, the use of variable optical attenuators or the previously mentioned Clos network with a specific connection pattern [8] can further decrease the path dependent loss if desired.
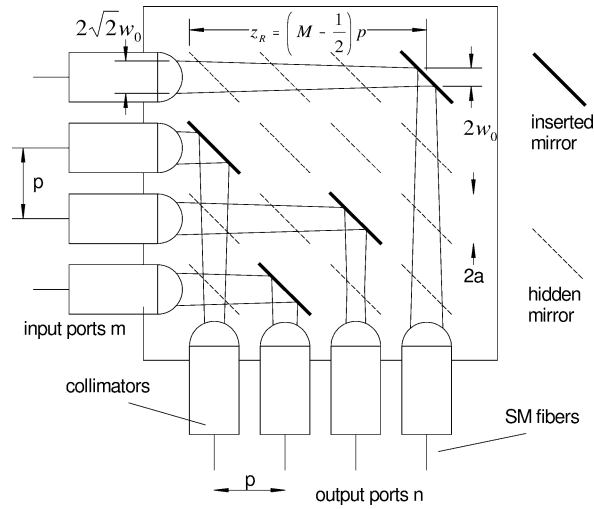
Fig. 1. Schematic drawing of a 4 × 4 freespace cross bar switch with $L_{\max} = 2z_R$.

There is no fundamental limit to scale up the single stage free-space cross-bar to any size at excellent optical performance when the design criteria given above are considered. However, the cross-bar switch gets less attractive at large port numbers due to the fast increasing size of the matrix and the required number of switching elements. In addition, larger switches with less divergent beams impose tighter angular tolerances on the optical parts [9]. Misalignment due to manufacturing errors or thermal expansion can not be compensated, due to the digital nature of the switching elements, which only can be positioned in the bar or cross state. Packaging issues are considered as the main reason why devices with port counts of $M > 32$, which are compliant to Telcordia Technologies environmental and reliability requirements, are not available to date.

## 4. The beam-steering free-space switch

The *beamsteering optical freespace switch* links a number of optical input ports with an equal number of optical output ports. The optical ports are, in most cases, end-faces of single-mode fibres or waveguides. The connection is established using focussing and moving optical elements placed in the free-space beam path. In general, two moving elements are used in a single path, with the first pointing the beam to the correct output port and the second redirecting the beam with the correct angle into the output fibre. An $M \times M$ switch therefore requires $NSE_{\mathrm{fs}} = 2M$ switching elements. The control of each switch element is usually analogue allowing to reach $M$ distinct positions required for path connection.

The free-space beam-steering switch seems to scale up to virtually unlimited number of ports [3]. However, there exists a maximum space available in typical telecommunication rack, which will limit the ultimate port number of such type of switches. In order to calculate the scalability of the switch, it is necessary to calculate the maximum number of ports for a given volume $V = L \times D_x \times D_y$. An arbitrary phase changing element with zero thickness is supposed to be located in the emitting and receiving planes in order to simplify the calculations and to give a most general model (Fig. 2). The phase changing elements are dynamic with respect to beam steering but fixed with a single focus length for coupling to the single-mode fibers outside of the emitting and receiving planes. The maximum path length $L_{\max}$ is set to $2z_R$, similar to the preceding chapter, and the beam waist $w_0$ is located in the center between the emitting and receiving planes. The loss and crosstalk are defined by the clipping ratio of the optical beam at the in and output ports. The following calculations all suppose a sufficient size of the beam using $a/w(z_R) = \pi/2$ similar to the preceding chapter.

We performed simple calculations based on Gaussian optics (see Appendix A) and obtained the maximum port number $M(Ra)$ as a function of the ratio $Ra = D/L$ (in the case of quadratic arrays with $D = D_x = D_y$) and the one-dimensional filling factors $f_{x,y} = 2a_{\mathrm{coll}}/p_{x,y}$, defined similar to the preceding chapter. Depending on the arrangement of the 2D array of collimators in the emitting and receiving plane, $f$ can reach $f_x = f_y = 1$ and $f_x = 1$, $f_y = 2/\sqrt{3}$ in the cubic and hexagonal closed-packed arrangement respectively. Eq. (5) results from equations (A.8) in Appendix A defining $F(Ra)$:

$$M(Ra, D) \cong \frac{f_x f_y}{\pi} \cdot \frac{D}{\lambda} \cdot F(Ra) + \frac{f_x + f_y}{\sqrt{\pi}} \cdot \sqrt{\frac{D}{\lambda}} \cdot \sqrt{F(Ra)} + 1 \tag{5}$$
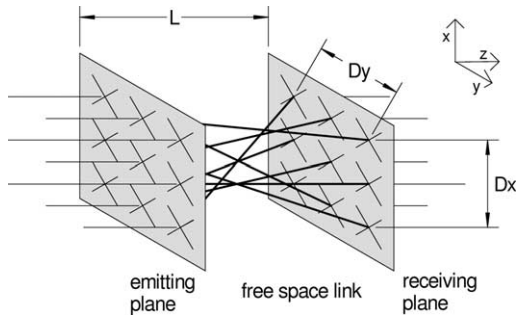
Fig. 2. Schematic drawing of a beamsteering freespace switch with arbitrary thin phase changing elements located in the emitting and receiving planes.
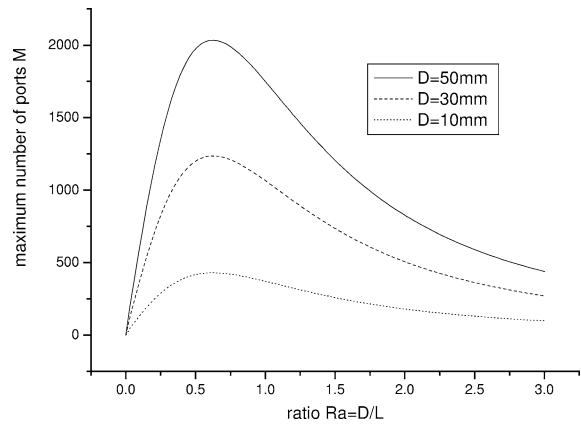


Fig. 3. Maximum achievable number of ports for a given 3D freespace switching volume $V = L \times D^2$ supposing a filling factor of $f_x = f_y = 0.75$ and $\lambda = 1.54$ μm.

with

$$F(Ra) = \frac{Ra}{\sqrt{1 + 2Ra^2(1 + Ra^2)}}.$$

Fig. 3 shows a plot of the maximum available port number $M(Ra, D)$ for different switching volumes $L \times D \times D$ and ratios $Ra$. The filling factors have been set to $f_x = f_y = 0.75$ reflecting actual constraints in micro optics and MEMS technology. The result shows that $M(Ra, D)$ exhibits a maximum for a certain geometry, namely for $Ra = D/L \approx 0.6$ with the corresponding maximum optical deflection angle $\alpha_{x,y} = 31°$. The assumption $L_{max} = 2z_R$ leads to a maximum spot size variation in the receiving plane of below $w_{max}/w_{min} < \sqrt{2}$. The corresponding path dependent coupling loss to the fibre is ca. $IL \approx 0.5$ dB supposing an ideal lens and neglecting phase terms in the overlap integral. A less compact design with $Ra < 0.6$ can further decrease the path dependent loss if desired.

The 3D freespace beamsteering switch can be scaled up to any port size without penalty in optical performance when the design criteria given above are considered. Contrary to the free-space cross-bar switch, the scaling laws are advantageous with respect to the number of switching elements NSE and required space, such that $M = 2025$ ports fit in $V = 38 \times 50 \times 50$ mm$^3$ ($f = 0.75$). In addition, assembly tolerances are less stringent, because the analogue beam-steering elements can actively compensate for alignment errors during operation. The limiting factor in three dimensional switches will be the precise control of the beam-steering elements, usually requiring additional sensors for feedback. The angular beam pointing tolerance can be calculated neglecting phase terms in the overlap integral. The result is given in Eq. (6) using a 0.5 dB coupling loss criteria. The switch mentioned above with 2025 ports therefore requires an angular positioning accuracy of better than $\alpha_{tol} = 0.06°$ over the whole switching range of $\alpha_{x,y} = 31°$. It is likely that the control electronics will fill up a telecommunication rack with increasing $M$ much faster than the space required for the optical switch itself. In addition, larger port counts, and the corresponding increase in size of the optical parts require high-quality optics and flat mirrors if MEMS are used. Increase in size of the movable optical parts usually decreases the switching speed, which also might be a limiting factor. For calculating the total switching speed, it has to be taken into account that that the first $M$ switching elements close to the emitting plane must be reconfigured before the second $M$ switching elements can be moved. If this rule is obeyed, it can be excluded that beams couple into unwanted configured output ports during switching.

$$\alpha_{tol} = \arg\tan\left(0.11 \frac{Ra \cdot f}{\sqrt{M} - 1}\right) \tag{6}$$

All considerations up to now are based upon an arbitrary phase changing element with zero thickness with the key function of collimating and beam-steering. Usually, this function can be fulfilled with different approaches. One possibility is to steer the beam by moving a lens in front of the input fibre and by pointing the beam in direction of the selected output port [12]. This solution can be very compact with a minimum of optical parts to be used. However, moving the lens out of the optical axis, which is fixed by the position of the fibers, will lead to coupling losses due to aberrations and the filling factor $f$ must be reduced in order to get the necessary space for the lateral movement of the lenses. Eq. (5) is still valid with $f \leqslant f(Ra)$ and an optical performance that decreases with larger port counts.

A better solution with respect to optical performance is to tilt the whole collimator [13] including the fiber. This solution leads to typically extremely low losses of <1 dB for all ports independent from port numbers. Concerning the filling factor, the

increased length of the collimators at higher port counts has to be taken into account, which require more space for tilting the collimators within the array. In addition, the increased size and weight of the movable parts will strongly influence the switching speed.

The most common solution uses *gimbal-mounted* mirrors as beam-steering elements and separate collimator arrays opposing the mirror arrays [3]. The mirror and collimator arrays are usually arranged in a so called *z*-design with two opposing mirror arrays and two collimator arrays that are arranged in a *z*-shape. The collimator array must be positioned far enough from the mirror array, in order not to obscure any beam within the switching volume. The optimum shape of the '*z*' depends mainly on the available tilt range of the mirrors and the filling factor. The resulting total optical path length is increased by a factor of up to three. The increased path-length will reduce the number of achievable ports for a given volume. A general model for the *z*-type switch has not yet been developed. Concerning a specific geometry, numerical simulations based on the ABCD method are presented in reference [14]. An analytical model of a *z*-shaped confocal 3D MEMS switch with different design criteria, especially with respect to clipping, is given in reference [15].

## 5. Conclusion

The scaling behaviour of different types of photonic switches based on optical path switching have been analysed. The main design rules for the free-space switches are defined, allowing to scale up the switches to any port number at a fixed level of insertion loss. Figs. 4 and 5 resume the main scaling behaviour of three photonic switch categories in a graphical representation using the equations provided in the text.

In Fig. 4, the tree architecture switch (a) supposes a size of the $1 \times 2$ elementary switch of 50 μm × 50 μm with $f = 0.75$ and enough space for the optical interconnects in between. The loss of a single $1 \times 2$ switch is set to 0.1 dB. The calculation of the minimum footprint of the freespace crossbar switch (b) results from Eq. (4). The footprint of the 3D beam-steering switch (c) results from Eq. (5) solving the equation with respect to $D^2$ and setting $Ra = 0.6$. The additional space required for the collimators is not taken into account for (b) and (c). The filling factors are set to $f = 0.75$. The insertion loss of $IL \leqslant 0.5$ dB results from the constant clipping ratio $a(z)/w(z) = \pi/2$, $L_{\max} = 2z_R$ and the path dependent losses.

In Fig. 5, the SN three-stage Clos architecture with 2 sets of $n \times k$ switches ($2kM$ switch elements) and one set of $M/n \times M/n$ ($k(M/n)^2$ switch elements) switches is optimised with respect to the minimum total number of switch elements. As a result, $k$ is set to $2n$ in order to be strictly nonblocking, and $n^2$ is set to $n^2 = M/2$.

The strongest increase in footprint shows the single stage free-space cross-bar switch (Fig. 4). Large port counts can not be reached without reduction in optical performance. A multistage design using a loss-homogenised Clos architecture is preferable, also with respect to packaging issues.

Concerning the tree architecture waveguide switch, acceptable footprints can be achieved with sufficiently small size of the elementary switch ⩽50 μm × 50 μm and interconnects with space requirements, which do not reduce the filling factor much less than $f < 0.75$. The total insertion loss also can be kept in an acceptable range, if the loss of the single switch element does not show more than 0.1 dB including the interconnects. For this type of switch, it is crucial that optical losses at optical crossings do not exist at all. The key limiting factor of the tree architecture is the huge number of switching elements required for switches with larger port counts, e.g., $M = 32$ already requires nearly 2000 elements. Even though the power consumption of a photonic
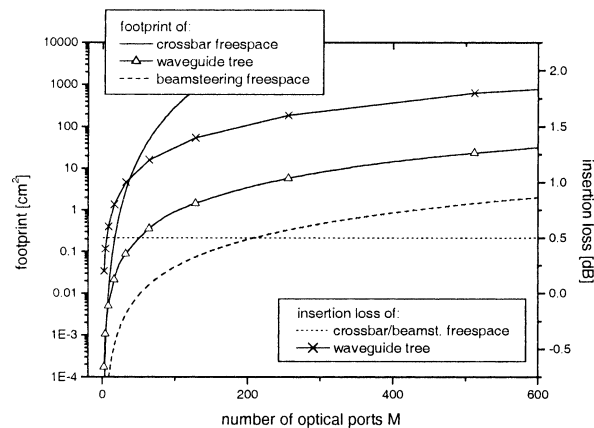


Fig. 4. Comparison of (a) the waveguide tree architecure switch; (b) the freespace crossbar switch; and (c) the 3D freespace beamsteering switch with respect to insertion loss and minimum required footprint versus port number $M$.
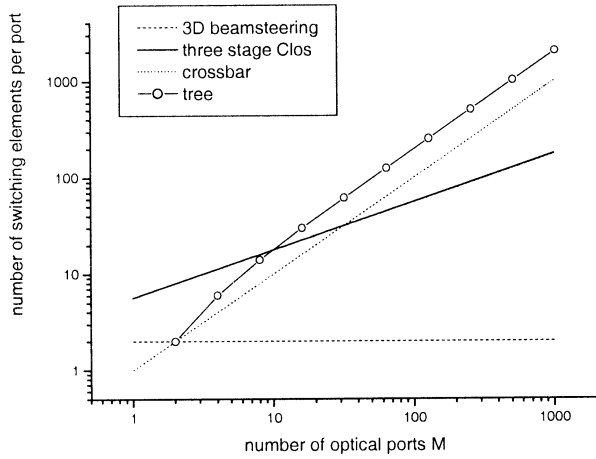
Fig. 5. The complexity of strictly nonblocking single stage beamsteering, crossbar and tree architectures is compared to the complexity of a three stage Clos architecture.
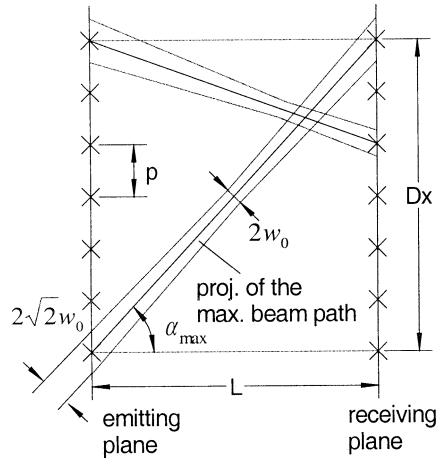


Fig. 6. Projection of the beam path with the maximum length $L_{\max}$ in the $y$–$z$ plane.

switch element might be very small, an unacceptable value of total power consumption can be reached fast at increased values of $M$.

The free-space beam-steering switch shows the best performance with respect to all criteria. A fully transparent switch ($IL < 0.5$ dB) with a maximum port number $M \approx 10^4$ can fit inside a telecommunication rack with $L \times D \times D = 83 \times 50 \times 50$ cm$^3$. This value will not be reached in reality because additional space for the collimators and the switch elements have to be taken into account. In addition, electronics and sensors that allow to keep the pointing accuracy of the beam-steering elements within $\alpha_{\text{tol}} < 0.03°$ ($M = 10^4$) over 31° switching range probably will not fit inside the rack. However, the potential of this technology with respect to massive transparent wavelength switching has been shown.

As mentioned before, carriers prefer to install equipment that is future proof and might be scaled up to higher data rates and higher port counts without exchanging the hardware. Adding any additional in and/or output port to the existing photonic switch requires full connectivity of the added port to the existing ports. This results in general in non-linear scaling laws of switching elements/interconnecting elements or crossings. The 3D free-space beam-steering switch behaves differently. Full interconnectivity to all added ports can be guaranteed without blocking, simply providing the required free-space volume in advance and respecting some additional rule (e.g., the scan angle and positioning accuracy of the switching elements must comply with the requirements of the final fully-populated switch). The 3D switch elements, the electrical interconnects and the optical platform also have to be prepared for adding additional ports. However, if these constraints have been considered, the port numbers of the switch can be increased by adding collimators, fibres, connectors, monitors and switching elements proportional to the added port numbers. Therefore, supposing that the assembly effort is not increased due to the increased number of installed optical elements, the costs of the photonic switch will scale linearly with the number of added ports, which seems not to be the case for any other type of switches. The price per port can even decrease at larger port counts, if batch fabrication of the optical parts and/or beam-steering elements in array form can be used. This is in general the case using MEMS technology or standard micro optics fabrication methods.

## Appendix A

The basic arrangement of Fig. 2 will be considered in the following calculations. All input beams can be directed to any output port with a maximum deflection angle $\alpha_{\max}$. The in- and output ports are located in coplanar planes with side lengths $D_x$, $D_y$ each and a distance $L$ between the planes. The origin of the $z$-axis is located in the centre between the planes. The beam intensity profile $I(r, \bar{z})$ emitted from optical ports (fibres) is assumed to be Gaussian-like. The following rules are thus applicable, with $r$ = radial distance from the optical axis, $\bar{z}$ = propagation length along the optical axes, $w_0$ = minimum waist of beam at $\bar{z} = 0$ and $z_{\text{R}}$ = Rayleigh range (defined by $w(z_{\text{R}}) = \sqrt{2}w_0$):

$$I(r, \bar{z}) = I_0(\bar{z})\, e^{-2r^2/w(\bar{z})^2}, \qquad (A.1)$$

$$w^2(\bar{z}) = w_0^2\left[1 + \left(\frac{\lambda \bar{z}}{\pi w_0^2}\right)^2\right], \qquad (A.2)$$

$$z_{\mathrm{R}} = \frac{\pi w_0^2}{\lambda}. \tag{A.3}$$

A free-space optical link with maximum distance and minimum waist is obtained for $L_{\max} = 2z_{\mathrm{R}}$ with the waist being centred between the optical ports at $z = 0$. In this idealised model, we assume that the beam waists located in the $x$–$y$-planes of the optical ports at $z = \pm L/2$ are correctly shaped to $w(z_{\mathrm{R}} = L_{\max}/2) = \sqrt{2}w_0$ with the corresponding wavefront curvature. Radial beam clipping is chosen to be defined by $r_{\mathrm{clip}} = \pi/2w(z_{\mathrm{R}})$. This value results in a relative power loss of $\Delta P/P = 0.72\%$ in the aperture plane and a maximum modification of the far-field beam divergence after the aperture of about 10% [11].

In the following, we consider a regular grid matrix of the optical input and output ports. For our calculations on the scalability, we define the one-dimensional filling factors $f_{x,y} = 2a_{x,y}/p_{x,y}$ with $p_{x,y}$ being the pitch in $x$ and $y$ direction respectively. The aperture $a_{x,y}$ can be elliptical and must satisfy the clipping condition. Actuation will be in general uncoupled in two orthogonal axes (e.g., using gimbal-mounted lenses or micro-mirrors). We therefore define the maximum angular deflection of the beam with respect to the orthogonal of the $x$–$y$-plane for the $x$–$z$- and $y$–$z$-planes independently:

$$\alpha_{x,y}^{\max} = \arctan\left(\frac{D_{x,y}}{L}\right) = \arcsin\left(\frac{D_{x,y}}{\sqrt{L^2 + D_{x,y}^2}}\right). \tag{A.4}$$

The optical axes of the beam is tilted with respect to the $x$, $y$ plane if $\alpha_{x,y} \neq 0$. The projection of the beam at the input/output ports at $z = \pm L/2$ represents a conic section of the beam, i.e., an ellipse. We suppose an uniform size of all ports (e.g., lenses or mirrors). Hence, the minimum dimensions of the input/output ports that guarantee the reflection/deflection of the total beam in all switching configurations, reads for $L \gg w_0$:

$$a_{x,y} = \frac{\sqrt{2}\pi w_0}{\cos \alpha_{x,y}^{\max}}. \tag{A.5}$$

The minimum pitch thus becomes

$$p_{x,y} = \frac{\sqrt{2}\pi w_0}{f_{x,y} \cos \alpha_{x,y}^{\max}} = \frac{\sqrt{2\pi \lambda z_{\mathrm{R}}}}{f_{x,y} \cos \alpha_{x,y}^{\max}} = \frac{\sqrt{\pi \lambda L_{\max}}}{f_{x,y} \cos \alpha_{x,y}^{\max}}. \tag{A.6}$$

We are interested in the scalability of the optical free-space switch, i.e., in the dependence of the maximum port number on the device dimensions. The maximum number of ports for a given switching volume $V = L * D_x * D_y$ can be written:

$$M = \left(\mathrm{mod}\left\{\frac{D_x}{p_x}\right\} + 1\right)\left(\mathrm{mod}\left\{\frac{D_y}{p_y}\right\} + 1\right) = \left(\mathrm{mod}\left\{\frac{f_x \cos \alpha_x^{\max} D_x}{\sqrt{\pi \lambda L_{\max}}}\right\} + 1\right)\left(\mathrm{mod}\left\{\frac{f_y \cos \alpha_y^{\max} D_y}{\sqrt{\pi \lambda L_{\max}}}\right\} + 1\right), \tag{A.7}$$

where mod denotes the *modulo* operator. For simplicity we consider quadratic micro-mirror arrays with $D = D_x = D_y$. Introducing the ratio $Ra = D/L$ and using the identity $\arcsin x = \arccos \sqrt{1 - x^2}$, the cosine of the maximum deflection angle becomes $\cos \alpha_{x,y}^{\max} = 1/\sqrt{1 + R^2}$. The maximum value of $M$ at a given geometry with $L_{\max} = \sqrt{L^2 + 2D^2}$ now becomes:

$$M \leqslant \left(\frac{f_x}{\sqrt{\pi}} \cdot \sqrt{\frac{D}{\lambda}} \cdot \sqrt{\frac{Ra}{\sqrt{1 + 2Ra^2}(1 + Ra^2)}} + 1\right) \cdot \left(\frac{f_y}{\sqrt{\pi}} \cdot \sqrt{\frac{D}{\lambda}} \cdot \sqrt{\frac{Ra}{\sqrt{1 + 2Ra^2}(1 + Ra^2)}} + 1\right). \tag{A.8}$$

## References

[1] A. Jourdan, F. Masetti, M. Garnot, G. Soulage, M. Sotom, J. Lightwave Technol. 14 (1996) 1198–1206.
[2] H.T. Mouftah, J.M.H. Elmirghani (Eds.), Photonic Switching Technology: Systems and Networks, Wiley–IEEE Press, 1998.
[3] R. Ryf, J. Kim, J.P. Hickey, A. Gnauck, D. Carr, F. Pardo, C. Bolle, R. Frahm, N. Basavanhally, C. Yoh, D. Ramsey, R. Boie, R. George, J. Kraus, C. Lichtenwalner, R. Papazian, J. Gates, H.R. Shea, A. Gasparyan, V. Muratov, J.E. Grifiith, J.A. Prybyla, S. Goyal, C.D. White, M.T. Lin, R. Ruel, C. Nijander, S. Arney, D.T. Neilson, D.J. Bishop, P. Kolodner, S. Pau, C. Nuzman, A. Weis, B. Kumar, D. Lieuwen, V. Aksyuk, D.S. Greywall, T.C. Lee, H.T. Soh, W.M. Mansfield, S. Jin, W.Y. Lai, H.A. Huggins, D.L. Barr, R.A. Cirelli, G.R. Bogart, K. Teffeau, R. Vella, H. Mavoori, A. Ramirez, N.A. Ciampa, F.P. Klemens, M.D. Morris, T. Boone, J.Q. Liu, J.M. Rosamilia, C.R. Giles, in: Proc. Optical Fiber Com. Conf. (OFC '01), Optical Society of America, Washington, DC, 2001, Paper PD28.
[4] A. Jajszczyk, H.T. Mouftah, IEEE Netw. 9 (1995) 10–16.
[5] N. Keil, H.H. Yao, C. Zawadzki, K. Satzke, W. Wischmann, J.V. Wirth, J. Schneider, J. Bauer, M. Bauer, in: Proc. Optical Fiber Com. Conf. (OFC '01), Optical Society of America, Washington, DC, 2001, Paper WR2.
[6] J.-P. Faure, L. Noirie, in: Proc. Optical Fiber Com. Conf. (OFC '01), Optical Society of America, Washington, DC, 2001, Paper WX5.
[7] F. Dorgeuille, L. Noirie, J.-P. Faure, A. Ambrosy, S. Rabaron, F. Boubal, M. Schilling, C. Artigue, in: Proc. Optical Fiber Com. Conf. (OFC '00), Optical Society of America, Washington, DC, 2000, Paper PD18.

 [8] G. Shen, T.H. Cheng, S.K. Bose, C. Lu, T.Y. Chai, J. Lightwave Technol. 20 (2002) 178–187.
 [9] L.-Y. Lin, E.L. Goldstein, R.W. Tkach, J. Lightwave Technol. 18 (2000) 482–489.
[10] H. Kogelnik, T. Li, Appl. Opt. 5 (1966) 1550–1567.
[11] P. Belland, J.P. Crenn, Appl. Opt. 21 (1982) 522–527.
[12] H. Toshiyoshi, J.G.-D. Su, J. LaCosse, M.C. Wu, in: Proc. IEEE Int. Conf. on Micro Opto Electro Mechanical Systems (MOEMS '99), IEEE, 1999, pp. 165–170.
[13] B.H. Lee, R.J. Capik, in: Proc. European Conference On Optical Communication (ECOC '00), Vol. 4, 2000, Paper 11.2.3.
[14] R.R.A. Syms, in: Proc. IEEE/LEOS Int. Conf. on Optical MEMS, IEEE, 2002, Paper WP31.
[15] P.M. Hagelin, U. Krishnamoorthy, J.P. Heritage, O. Solgaard, IEEE Photon. Technol. Lett. 12 (2000) 882–884.